BMC Cardiovascular Disorders

RESEARCH

Open Access

Exosomes activate hippocampal microglia in atrial fibrillation through long-distance heart–brain communication

Xuewen Wang[1,2,3,4†], Yuanjia Ke[1,2,3†], Zhen Cao[1,2,3†], Yuntao Fu[1,2,3], Yanni Cheng[1,2,3], Dishiwen Liu[1,2,3], Huiyu Chen[1,2,3], Kexin Guo[1,2,3], Yajia Li[1,2,3], Mei Yang[1,2,3*] and Qingyan Zhao[1,2,3*]

Abstract

Background There is growing evidence that atrial fibrillation (AF) is a risk factor for cognitive impairment (CI) and dementia in the presence or absence of stroke. The purpose of this study was to explore the mechanism of CI caused by AF.

Methods Eighteen male canines were randomly divided into a sham group, a pacing group, and a pacing + GW4869 group. An experimental model of AF was established by rapid atrial pacing (450 beats/min) for 2 weeks, and the sham group received pacemaker implantation without atrial pacing. The GW4869 group received an intravenous GW4869 injection (0.3 mg/kg, once a day) during pacing. All canines were locally injected with Ad-CD63-RFP in epicardial adipose tissue (EAT) to trace the exosomes. Ultracentrifugation was employed to isolate EAT-derived exosomes, followed by RNA sequencing and quantitative real-time PCR (qRT-PCR) to assess RNA in both exosomes and hippocampal tissue. The miRanda database was used to predict the targeting relationships between miRNA and mRNA, which were further validated by luciferase reporter assays. Western blot analysis was conducted to detect exosomal markers (CD63, CD81, TSG101) in EAT exosomes, while immunofluorescence was used to detect Ad-CD63-RFP signals in both EAT and hippocampal tissues, as well as microglial activation marker IBA-1. To further explore the effects of exosomes on microglial cells, in vitro experiments using brain microvascular endothelial cells (bEnd3) and microglial cells (BV2) were conducted. IBA-1 expression and RNA levels in BV2 cells were analyzed by immunofluorescence and qRT-PCR, respectively.

Results After 14 days of pacing of the canine atrium, compared to the sham group, both the pacing and GW4869 groups exhibited an increased number of AF inductions, along with prolonged AF duration. The fluorescence intensity of Ad-CD63-RFP and the microglial activation marker IBA-1 were markedly greater in the hippocampus. RNA sequencing showed that the differentially expressed gene cfa-miR-22e in EAT exosomes was upregulated, and

†Xuewen Wang, Yuanjia Ke and Zhen Cao contributed equally to this work and are co-first authors.

*Correspondence:
Mei Yang
rm002693@whu.edu.cn
Qingyan Zhao
ruyan71@163.com

Full list of author information is available at the end of the article

its target gene IL33 was downregulated in the hippocampus. qRT-PCR showed that the levels of cfa-miR-22e were increased in both EAT exosomes and the hippocampus, while the expression of IL-33, a target of cfa-miR-22e, was decreased in the hippocampus. The administration of GW4869 abolished these effects. The in vitro results from bEnd3 and BV2 cell experiments were consistent with the conclusions drawn from the in vivo studies.

Conclusion Our study indicated that the exosomes secreted by EAT in canines with AF can penetrate the BBB and activate microglia in the hippocampus through the cfa-miR-22e/IL33 signalling pathway.

Keywords Atrial fibrillation, Exosomes, Cognitive impairment, Microglia, Canine

Introduction

Atrial fibrillation (AF) is the most common type of arrhythmia worldwide, and cognitive impairment (CI) is one of the serious complications of AF [1, 2]. In 1977, Ott et al. first reported that arrhythmia can increase the risk of cognitive impairment [3], and a systematic review and meta-analysis suggested that AF may be associated with an increased risk of both CI and Alzheimer's disease in a broad population [4]. Stroke, cerebral small vessel disease and cerebral hypoperfusion are considered to be important causes of AF-associated CI [5, 6]. However, clinical studies have shown that there are no significant differences in cerebral small vessel disease between AF patients and non-AF patients [7, 8]. Recent studies have also shown that AF has little effect on regional cerebral blood flow in patients with Alzheimer's disease [9]. To date, the exact mechanism by which AF increases the risk of CI remains unclear.

Recent research has suggested that glial cells (especially microglia) may cause neuronal damage through the release of inflammatory factors and chemokines, adhesion and invasion, and oxidative stress and increase the risk of pathological changes related to CI. Intervention in the activation of microglia can reduce neuroinflammation and improve CI [10, 11]. Exosomes are 40–150 nm small extracellular vesicles secreted by most cells, and RNA (including mRNA, miRNA, and other noncoding RNA), proteins, and lipids are selectively incorporated into exosomes and then released into the extracellular space [12]; these vesicles are involved in cell signalling, cell differentiation, immune regulation, substance metabolism and gene regulation and carry proteins and RNA that can be inserted into recipient cells to induce short- or long-term phenotypic changes [13]. Epicardial adipose tissue (EAT) of patients with AF can release a large number of exosomes [14], and the direct transfer of exosomal miR-1 from the heart to the hippocampus may lead to microtubule damage in the hippocampus [15]. Other studies have shown that microRNAs (miRNAs) play a proinflammatory role in the activation of microglia and participate in the activation of microglia by inhibiting anti-inflammatory-related proteins [16, 17]. However, it is unclear whether the cognitive dysfunction caused by AF is related to the activation of microglia by EAT-derived exosomes. This study explored the potential mechanism by which EAT-derived exosomes increase the risk of cognitive impairment in AF.

Materials and methods

Animal preparation

All animal experiments were conducted in accordance with the Guide for the Care and Use of Laboratory Animals of the US National Institutes of Health and were approved by the Animal Ethics Committee of Renmin Hospital at Wuhan University. Eighteen male beagle canines weighing 10 to 15 kg were used in this experiment and maintained under the same conditions in the Animal Experimental Center of Renmin Hospital of Wuhan University. After one week of acclimatization, the canines were randomly assigned to three groups (n=6 for each group). The sham group received pacemaker implantation without atrial pacing. The pacing group received pacemaker implantation with continuous rapid atrial pacing (450 beats/min) for 2 weeks, the pacing parameters were determined based on previous research experiences [18]. The GW4869 group underwent the same pacing model as the pacing group and was administered a slow intravenous injection (0.3 mg/kg, once a day) of GW4869 (MedChemExpress, USA), the injection dose was based on our experience from previous studies [19]. All canines were injected with Ad-CD63-RFP (DesignGene Co., Ltd., Shanghai, China) at multiple EAT points in the left atrial free wall to trace the exosomes. Pacing was measured 3 days after pacemaker implantation in the pacing group and GW4869 group. The canines were euthanized by air embolism at the end of the experiment.

Cardiac pacemaker implantation and administration

After anaesthesia with 3% pentobarbital sodium (30 mg/kg), the canines were trachea cannulated and ventilated with a positive pressure respirator (WATO EX-20Vet; Mindray, Shenzhen, China) with 2 L/min oxygen. The left atrial appendage and left atrial EAT were completely exposed through the left third intercostal space incision. The distal end of the bipolar pacing lead (QM7222-53; LEPU MEDICAL, Beijing, China) was secured to the left atrial appendage with cotton thread (5−0), and the proximal end of the pacing lead was connected to a rapid pulse

generator (Harbin University of Science and Technology, China), which was implanted into a submuscular pocket on the left side of the chest. After testing for normal atrial pacing function, the surgical incision was sutured layer by layer. Ad-CD63-RFP (100 μl of 1×10^{11} pfu/ml) was administered to all groups as described above. An intravenous infusion of saline was supplied to compensate for fluid loss during the procedure, and continuous ECG monitoring was performed by a computer-based multichannel electrophysiology system (Lead 7000, Jinjiang Inc., China). A 30-second single-lead ECG was monitored three times a week after the pacemaker was turned on to ensure that atrial pacing was normal.

All operations were performed under sterile conditions, and 100 mg/day ceftiofur sodium was intramuscularly injected for 7 days for prophylactic anti-infective treatment.

Cardiac electrophysiological measurement

At the end of the experiment (after two weeks of atrial pacing), we performed programmed stimulation on the left atrium (LA), left atrial appendage (LAA), and the left superior and inferior pulmonary veins (LSPV/LIPV) in each group of canines to assess AF inducibility. After preparing the canines in a manner similar to pacemaker implantation, we exposed these four anatomical sites and sutured the mapping/stimulation electrodes to these areas, ensuring proper display of atrial potentials. High-frequency S1S1 programmed stimulation was employed to test AF inducibility. The stimulation parameters were set as follows: S1S1 intervals of 120, 100, 75, and 60 ms, pulse width of 2 ms, and pacing voltage at the minimum pacing threshold, approximately 5 V. Each pacing cycle length was stimulated 3 times, with each stimulation lasting 5 s. AF was defined as the appearance of fibrillation waves in the atrial potentials recorded by the Lead7000 multi-lead electrophysiological system, with an atrial frequency > 500 beats per minute, irregular ventricular rhythms, and a duration exceeding 5 s. The number and duration of AF inductions were recorded.

Exosome isolation

Left atrial EAT samples from all groups of canines were obtained immediately after the canines were euthanized, rinsed with normal saline, and then stored in sterile cryopreserved tubes in liquid nitrogen until examination. The tissues were thawed in a 37 °C incubator, washed twice with PBS, cut into approximately 1 mm^3 tissue fragments, and placed in a 50 ml centrifuge tube. Then, 0.25% trypsin-EDTA (Gibco, 25200-072) was added to an equal volume, and the tissue was digested in a 37 °C incubator with slight shock for 2–3 hours until the cell suspension was milky. Digestion was terminated with DMEM containing 10% nonexosomal serum, the mixture was centrifuged at 2000 × g for 5 min, and the supernatant was collected. The exosomes were extracted from the supernatant by ultracentrifugation at 4 °C at 10,000 × g and 100,000 × g. The extracted exosomes were used for further detection.

RNA sequencing and data analysis

miRNA was detected in EAT exosomes from canines in the sham group and the pacing group, and mRNA was detected in hippocampal tissue from the same group of canines. Total RNA was extracted from EAT exosomes and hippocampal tissues using a Total RNA Kit (TIANGEN, DP761) according to the manufacturer's protocol and then qualified and quantified using a NanoDrop Onec spectrophotometer (Thermo Fisher Scientific Inc.) and a Qubit 3.0 with a Qubit™ RNA Broad Range Assay kit (Life Technologies, Q10210). Unique molecular identifier RNA-seq experiments and high-throughput sequencing were conducted by Seqhealth Technology Co., Ltd. (Wuhan, China). The differentially expressed miRNAs/mRNAs between groups were identified using the edgeR package (version: 3.12.1). Thresholds of $\log_2$_fold change (FC) > 1 and P value < 0.05 were used to determine the statistical significance of differences in RNA expression. The target miRNAs of the differentially expressed mRNAs were predicted with miRanda v3.3a.

Construction of adenovirus vectors

Ad-hCD63-mCherry (Ad-CD63-RFP) was designed by DesignGene (DesignGene Co., Ltd., Shanghai, China). The DNA sequences of primers used were as follows:

hCD63-NheI-Forward:

5'-CTAGCTAGCCACCATGGCGGTGGAAGGAGGAATGAAA-3';

hCD63-AscI-Reverse:

5'-ATTTGGCGCGCCTCATCACCTCGTAGCCACTTCTGATA-3'.

The adenoviral plasmid pDC315-hCD63-mCherry was transfected into HEK293 cells to obtain adenoviruses containing the target gene, labelled Ad-hCD63-mCherry. The viral particles were harvested at 48 h posttransfection. After purification and concentration, the recombinant adenovirus vectors were obtained at a titre of 1×10^{11} PFU/ml for injection.

Cell culture and in vitro treatments

Brain microvascular endothelial cells (bEnd.3) and microglial cells (BV2), both purchased from IMMOCELL (Xiamen, China), were cultured in high-glucose DMEM containing 10% fetal bovine serum and 1% penicillin/streptomycin (all from Gibco, USA) under standard conditions (37℃, 5% CO2, humidified incubator). bEnd.3 cells were used to simulate the blood-brain barrier (BBB), and bEnd.3 and BV2 cells were co-cultured in Transwell

plates (pore size 0.4 μm, diameter 11 mm; Corning, Lowell, MA, USA) to observe whether exosomes could penetrate the BBB and affect microglial activation (Fig. 2D). After 48 h of culture, the bEnd.3 cells fully covered the upper chamber, and the integrity of the BBB was verified using fluorescein isothiocyanate (FITC)-dextran (1 mg/mL, Sigma-Aldrich) [20]. Subsequently, exosomes isolated from the EAT of sham-operated and paced canines were added to the upper chamber bEnd.3 medium in the co-culture system. After an additional 48 h of co-culture, the BV2 cells in the lower chamber were collected for immunofluorescence analysis to evaluate the impact of exosomes on microglial activation. Next, BV2 cells were divided into four groups: control, mimics-NC, cfa-miR-22e-mimics, and cfa-miR-22e-inhibition, and cultured for 48 h. Lipofectamine 6000 (Beyotime, China) was used to transfect mimic-NC and cfa-miR-22e mimic/inhibitor, and cells were harvested after 24 h for further experiments. To verify the role of IL-33 in the cfa-miR-22e-mediated effects on microglial cells, additional groups were set up: control, mimics-NC, cfa-miR-22e-mimics, cfa-miR-22e-inhibitor, and cfa-miR-22e-mimics + IL-33 (MedChemExpress, USA). The mimics-NC (5'-UCACAACCUCCUAGAAAGAGUAGA-3'), cfa-miR-22e-mimics (5'-AGGAAGGUGGGGAUGAAG-3'), and cfa-miR-22e-inhibition (5'-CUUCAUCCCCACCUUCCU-3') were all synthesized by General Biol (China).

Quantitative real-time PCR analysis

Total RNA was isolated from EAT exosomes, hippocampal tissues, and BV2 cells using Total RNA Extraction Reagent (Servicebio, China) according to the manufacturer's protocols. The relative levels of cfa-miR-22e and IL33 were detected by stem–loop RT-qPCR using universal Blue SYBR Green qPCR Master Mix (Servicebio, China) with a real-time PCR instrument (Bio-Rad, USA). The data were analysed by the $2^{-\triangle\triangle CT}$ method. The primer sequences for qRT-PCR were as follows: cfa-miR-22e: 5'-ACACTCCAGCTGGGAGGAAGGTGGGG-3' (Forward), 5'-TGGTGTCGTGGAGTCG-3' (Reverse); IL33: 5'-AAGATTTCACCTCTGATGTCCCTA-3' (Forward), 5'-GGAATCATAATAACGGAATAACACC-3' (Reverse); canine-U6: 5'-CTCGCTTCGGCAGCACA-3' (Forward), 5'-AACGCTTCACGAATTTGCGT-3' (Reverse); and canine-GAPDH: 5'-GGGTGATGCTGGTGCTGAGTAT-3' (Forward), 5'-TTGCTGACAATCTTGAGGGAGTT-3' (Reverse).

Luciferase reporter assay

To validate that IL33 was a target gene of cfa-miR-22e, wild-type (wt) or mutant (mut) IL33 3'UTRs containing the binding site of cfa-miR-22e were synthesized, cloned and inserted into the pmirGLO reporter vector (Promega). cfa-miR-22e-mimics or miRNA-NC and wt-IL33 or mut-IL33 reporter constructs were cotransfected into cells with a Renilla luciferase vector. After 48 h of transfection, luciferase activities were determined by a dual-luciferase reporter assay system (Promega, United States).

Immunofluorescence

At the end of the experiment, the bilateral hippocampus, other parts of the brain and small portions of EAT from the free wall of the left atrium were quickly removed and washed with normal saline. The hippocampus and EAT were fixed with 4% paraformaldehyde and paraffin-embedded. BV2 cells were fixed with 4% paraformaldehyde before detection. For immunofluorescence staining, the deparaffinized sections were subjected to antigen retrieval. Hippocampal samples and BV2 cells were incubated with primary antibodies against IBA-1 (Abways, CY7217) and subsequently with the secondary antibodies CY3-conjugated AffiniPure goat anti-rabbit IgG and FITC-conjugated AffiniPure goat anti-rat IgG (Jackson, USA). Other parts of the brain tissue were taken to detect the fluorescence intensity of Ad-CD63-RFP. The nuclei were stained with DAPI, and the results were analysed by Image-Pro Plus 6.0 software (Media Cybernetics, USA). Three visual fields in each sample were assessed randomly at 400× magnification. The degree of tissue fluorescence was quantified by measuring the average optical density in the digitized images using the ImageJ program (National Institutes of Health, Bethesda, MD, USA).

Western blot analysis

Total protein was extracted from canine EAT. The protein concentration was determined by a BCA Protein Assay Kit (Beyotime, P0010S) according to the manufacturer's instructions. Proteins were separated on a 10% SDS–polyacrylamide gel and transferred to a 0.45 μM PVDF membrane. The experimental methodology is mainly based on the previous experience of our subject group [19]. The expression of target proteins was determined by incubating the membranes with the following primary antibodies overnight at 4 °C: CD63 (Servicebio, China), CD81 (Abcam, USA), TSG101 (Sigma–Aldrich, Germany), and GAPDH (Servicebio, China). Visualization was performed on a chemiluminescence system after incubation with horseradish peroxidase-conjugated secondary antibodies (Proteintech, China) at room temperature.

Statistical analysis

GraphPad Prism 9.0 software was used for statistical analysis. Normally distributed measurement data are represented as $\bar{x} \pm s$. Two-sample independent Student's t tests were performed to compare the means of two

groups. ANOVA followed by the Tukey–Kramer test was used to compare the mean values of continuous variables among multiple groups. All the statistical tests were two-sided, and a probability value <0.05 was regarded as statistically significant.

Results

The susceptibility to AF was increased in rapid atrial pacing canines

Programmed stimulation was used to evaluate AF induction at the LA, LAA, LSPV, and LIPV. Compared to the sham group, the pacing group and the pacing+GW4869 group exhibited a significant increase in AF induction frequency (1.00±0.82 vs. 5.17±1.07 and 4.17±1.06, respectively, $P<0.001$), along with a marked extension in AF duration (1.83±1.46 vs. 35.83±7.73 s and 28.17±5.40 s, respectively, $P<0.001$) (Fig. 1C, D). However, there was no statistically significant difference in the number of AF inductions or the duration of AF episodes between the pacing group and the pacing+GW4869 group.

Rapid atrial pacing increased the secretion of EAT exosomes

As shown in Fig. 2, the morphology and particle size were observed by transmission electron microscopy and nanoparticle tracking analysis (NTA), respectively. The size of the vesicles ranged between 30 and 150 nm, the mean size of which was 83.5 nm in diameter. After rapid atrial pacing, the concentration of EAT exosomes increased to $(1.92\pm0.13)\times10^{10}$ particles/ml from $(1.27\pm0.19)\times10^{10}$ particles/ml, which decreased to $(1.32\pm0.21)\times10^{10}$ particles/ml after GW4869 treatment (both $P<0.05$). The mean fluorescence intensity of Ad-CD63-RFP in the EAT of the pacing group was significantly greater than that in the sham group (35.7±2.4 vs. 10.2±2.1, $P<0.001$), which could be reversed by GW4869 treatment (35.7±2.4 vs. 14.7±2.0, $P<0.001$, Fig. 2C, D). Furthermore, western blotting revealed that the levels of exosome marker proteins (CD63, CD81, and TSG101) in the EAT were significantly greater in the pacing group than in the sham group (CD63: 0.63±0.03 vs. 0.24±0.05; CD81: 0.61±0.03 vs. 0.19±0.01, TSG101: 0.59±0.02 vs. 0.18±0.01) and the pacing+GW4869 group (CD63: 0.63±0.03 vs. 0.44±0.07; CD81: 0.61±0.03 vs. 0.39±0.02, TSG101: 0.59±0.02 vs. 0.36±0.03), both $P<0.001$

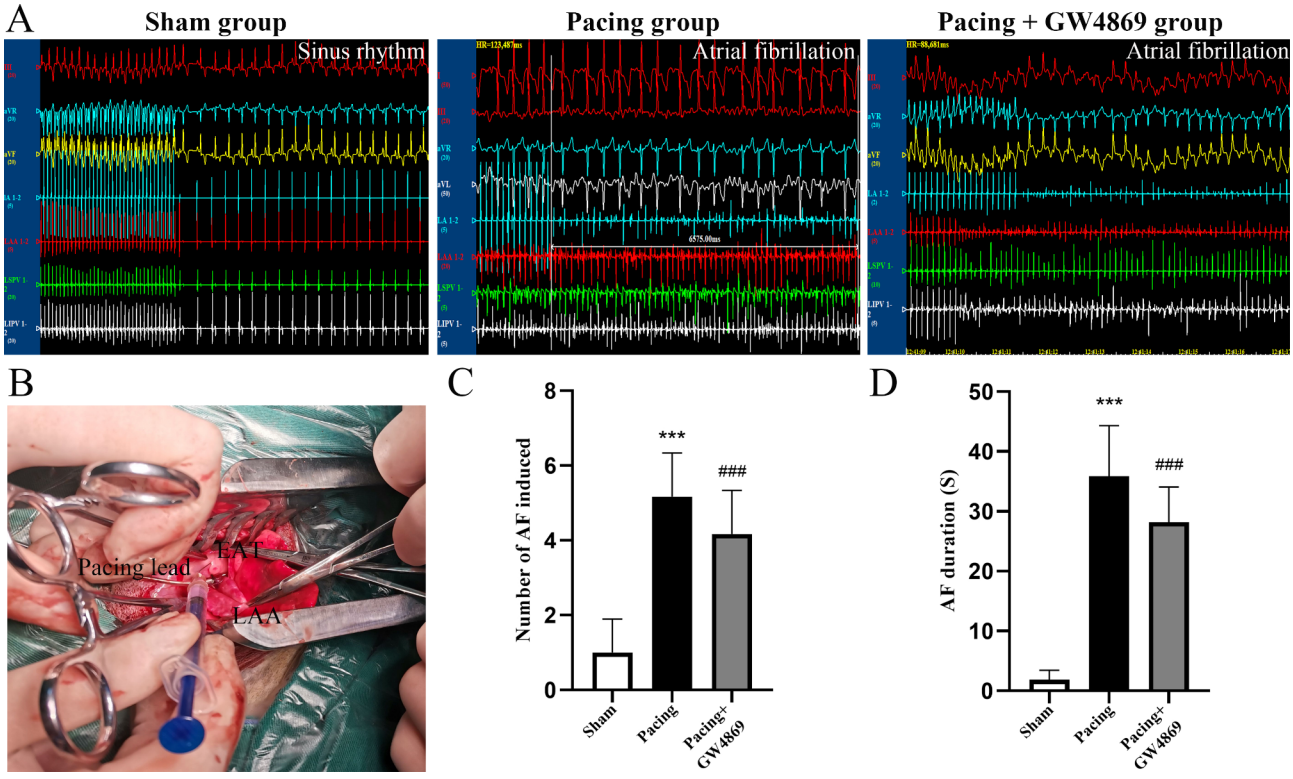

Fig. 1 (**A**) Representative images of AF induction via programmed stimulation in the three groups of canines. (**B**) Thoracotomy was performed at the third intercostal space of the left chest, with the pacing lead fixed at the LAA. Multiple injections of diluted Ad-CD63-RFP were made into the EAT on the free wall of the left atrium. (**C**, **D**) The average number of AF inductions and duration of sustained AF episodes in the three groups. Data are presented as the mean ± standard deviation from 6 canines in each group. Compared to the Sham group, ***$P<0.001$, ###$P<0.001$. There was no statistically significant difference between the Pacing group and the Pacing + GW4869 group. AF = atrial fibrillation; EAT = epicardial adipose tissue; LAA = left atrial appendage

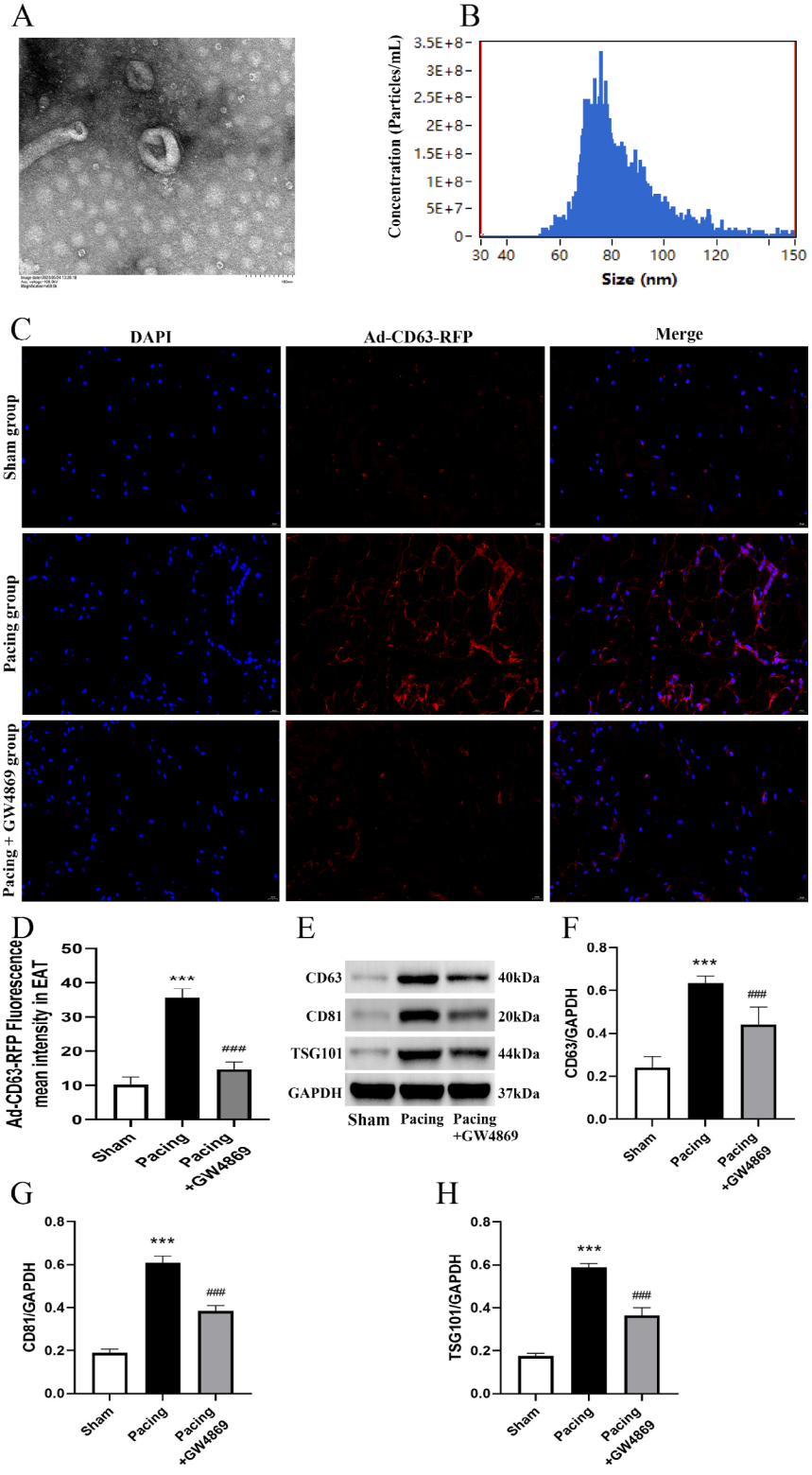

Fig. 2 Analysis of exosomes in the EAT of canines. (**A**) Representative electron microscopy image of exosomes isolated from EAT ($n=3$, scale bar, 100 nm). (**B**) Representative NTA image of the exosome size range and concentration ($n=3$; dilution ratio, 1:500). (**C**, **D**) Representative image of Ad-CD63-RFP immunofluorescence and the mean intensity of Ad-CD63-RFP in EAT ($n=6$, x400). (**E**) Representative western blotting images of CD63, CD81 and TSG101 in EAT. (**F**-**H**) The mean expression levels of CD63, CD81 and TSG101 in EAT ($n=6$ for each group). *** $P<0.001$ versus the sham group; ### $P<0.001$ versus the pacing group. EAT = epicardial adipose tissue; NTA = nanoparticle tracking analysis

(Fig. 2E-H). These results suggested that rapid atrial pacing significantly increases the release of EAT exosomes.

Rapid atrial pacing increased the distribution of EAT exosomes in the hippocampus

As shown in Fig. 3, to explore whether EAT-derived exosomes can enter the hippocampus through the BBB, we traced EAT-derived exosomes by local Ad-CD63-RFP injection. We found that the fluorescence intensity of the virus was markedly greater in the pacing group than in the sham group (20.2±1.7 vs. 9.2±1.6, $P<0.001$), while GW4869 treatment significantly reduced the expression of Ad-CD63-RFP in the hippocampus compared with that in the pacing group (20.2±1.7 vs. 11.6±1.9, $P<0.001$). The Ad-CD63-RFP fluorescent signals were distributed throughout the central nervous system in pacing canines, with the strongest intensity observed in the hippocampal region (Fig. 3C). We also constructed a bEnd.3 and BV2 cell coculture system. Viral fluorescence was detected in BV2 cells (Fig. 3D). Compared with that in the control group, the fluorescence intensity of the virus in BV2 cells increased significantly in the pacing group (11.6±1.9 vs. 37±2.8, $P<0.001$). The results indicated that EAT-derived exosomes could enter the hippocampus through the BBB.

Analysis of differentially expressed genes and miRNA–mRNA regulatory networks

We found 318 differentially expressed mRNAs in the hippocampus of the sham group and the pacing group, including 102 that were upregulated and 216 that were downregulated, and 13 differentially expressed miRNAs in EAT exosomes, including 11 that were upregulated and 2 that were downregulated. The raw transcriptome data were uploaded to the GEO database (GSE240776). The differentially expressed genes are illustrated in a heatmap and volcano plot (Fig. 4A-C). Table 1 lists the differentially expressed mRNAs associated with microglia and their targeted miRNAs. The targeted miRNA of hippocampal mRNA was predicted by miRanda and intersected with the miRNA of EAT exosomes, and a total of 10 intersecting genes were obtained (Fig. 4D). novel-22, a differentially expressed miRNA in EAT exosomes, was predicted using the miRanda database to possess multiple target binding sites on IL-33 mRNA, a gene linked to microglial activation. This miRNA, designated as cfa-miR-22e, has a mature sequence of AGGAAGGU GGGGAUGAAG.

Cfa-miR-22e targeted the IL33 gene and promoted the activation of microglia in the hippocampus

We next aimed to clarify whether IL33 is the target of cfa-miR-22e. By performing computational analysis of miRNA databases (miRanda), we found that cfa-miR-22e targets multiple sites of IL33 (Fig. 5, C). To validate this hypothesis, we performed a luciferase assay using wild-type and mutated nucleotide sequences of putative binding sites of the 3'UTR of IL33 on cfa-miR-22e. The results showed a significant reduction in the luciferase signal in 293T cells in the cfa-miR-22e-IL33 WT group (0.41±0.07, $n=5$) compared to that in the miRNA-NC-IL33 WT group (1.05±0.10, $n=5$, $P<0.001$) and the cfa-miR-22e-IL33 MUT group (1.00±0.10, $n=5$, $P<0.001$) (Fig. 5, D). To further explore the relationship between cfa-miR-22e and IL33, qRT-PCR was used to verify RNA expression in EAT exosomes and the hippocampus. As shown in Fig. 5E-G, compared with that in the sham group, the level of EAT exosomal cfa-miR-22e was significantly greater in the pacing group (0.98±0.11 vs. 4.05±0.17, $P<0.001$), and the administration of GW4869 reversed this effect (4.05±0.17 vs. 2.05±0.17, $P<0.001$). Moreover, the expression of cfa-miR-22e in the hippocampus was consistent with that in EAT exosomes. Furthermore, the expression level of IL33 in the hippocampus of the pacing group was lower than that in the sham group (0.98±0.11 vs. 3.05±0.17, $P<0.001$) and in the pacing+GW4869 group (0.98±0.11 vs. 1.9±0.13, $P<0.001$). To evaluate the degree of microglial activation in the hippocampus, we examined the microglial activation marker IBA-1 by immunofluorescence staining. As shown in Fig. 5A and B, immunofluorescence staining revealed that the density of IBA-1 was significantly greater in the pacing group than in the sham group (30.1±1.4 vs. 13.7±1.1, $P<0.001$) and was dramatically reduced by GW4869 treatment (30.1±1.4 vs. 22.3±1.1, $P<0.001$). These data illustrated that exosome-mediated microglial activation resulted from EAT exosomal cfa-miR-22e and its downstream IL33 pathway in a canine model of AF.

Effects of cfa-miR-22e and IL33 on microglial activation in vitro

To further explore the effect of cfa-miR-22e and IL33 on the activation of microglia, we performed BV2 cell experiments. Immunofluorescence showed that the mean fluorescence intensity of IBA-1 was significantly greater in the cfa-miR-22e-mimic group than in the control group, mimic-NC group and cfa-miR-22e inhibitor group (IBA-1: 44±1.6 vs. 10.3±1.5, 8.5±0.11, 8.5±1.2, $P<0.001$). qRT-PCR also revealed that the level of cfa-miR-22e in BV2 cells was significantly higher in the mimics group than in the control group, mimic-NC group and cfa-miR-22e inhibitor group (2.22±0.08 vs. 0.93±0.15, 0.85±0.11, 1.14±0.10, $P<0.001$), and the level of IL33 in BV2 cells was significantly lower in the mimics group than in the control group, mimic-NC group and cfa-miR-22e inhibitor group (0.17±0.02 vs. 0.80±0.08, 0.80±0.04, 2.43±0.12 $P<0.01$) (Fig. 6).

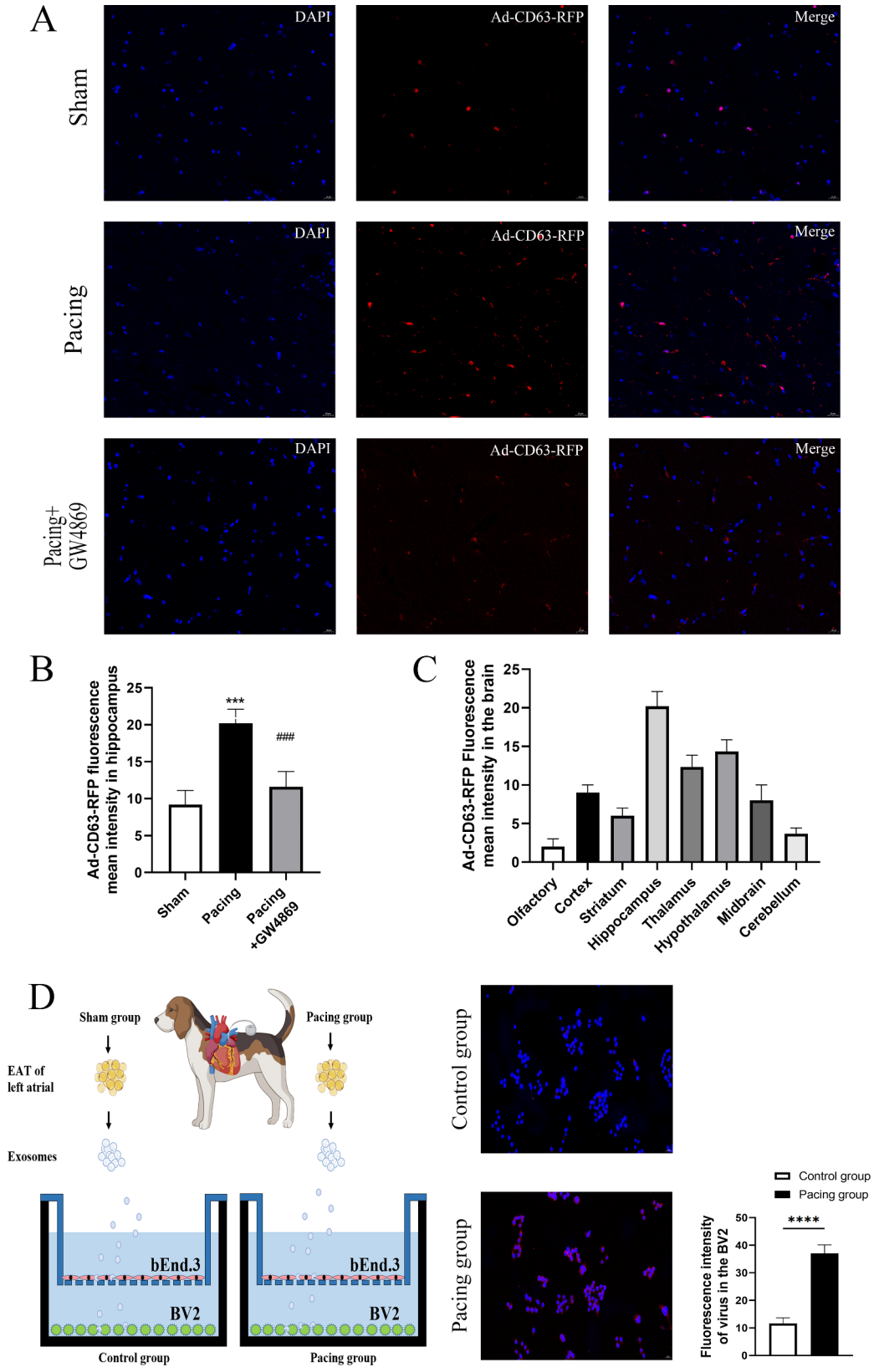

Fig. 3 Ad-CD63-RFP-labelled canine EAT exosomes penetrate the BBB. (**A**, **B**) Fluorescence mean intensity of Ad-CD63-RFP in the hippocampus of the three groups of canines. (**C**) Fluorescence mean intensity of Ad-CD63-RFP in different parts of brain tissue. (**D**) bEnd.3 cells mimic the BBB, exosomes isolated from the EAT of canines penetrate the BBB, and red fluorescence indicates Ad-CD63-RFP-labelled exosomes. *** $P < 0.001$ versus the sham group; ### $P < 0.001$ versus the pacing group; **** $P < 0.0001$ versus the control group. EAT = epicardial adipose tissue; Ad = adenovirus; BBB = blood brain barrier

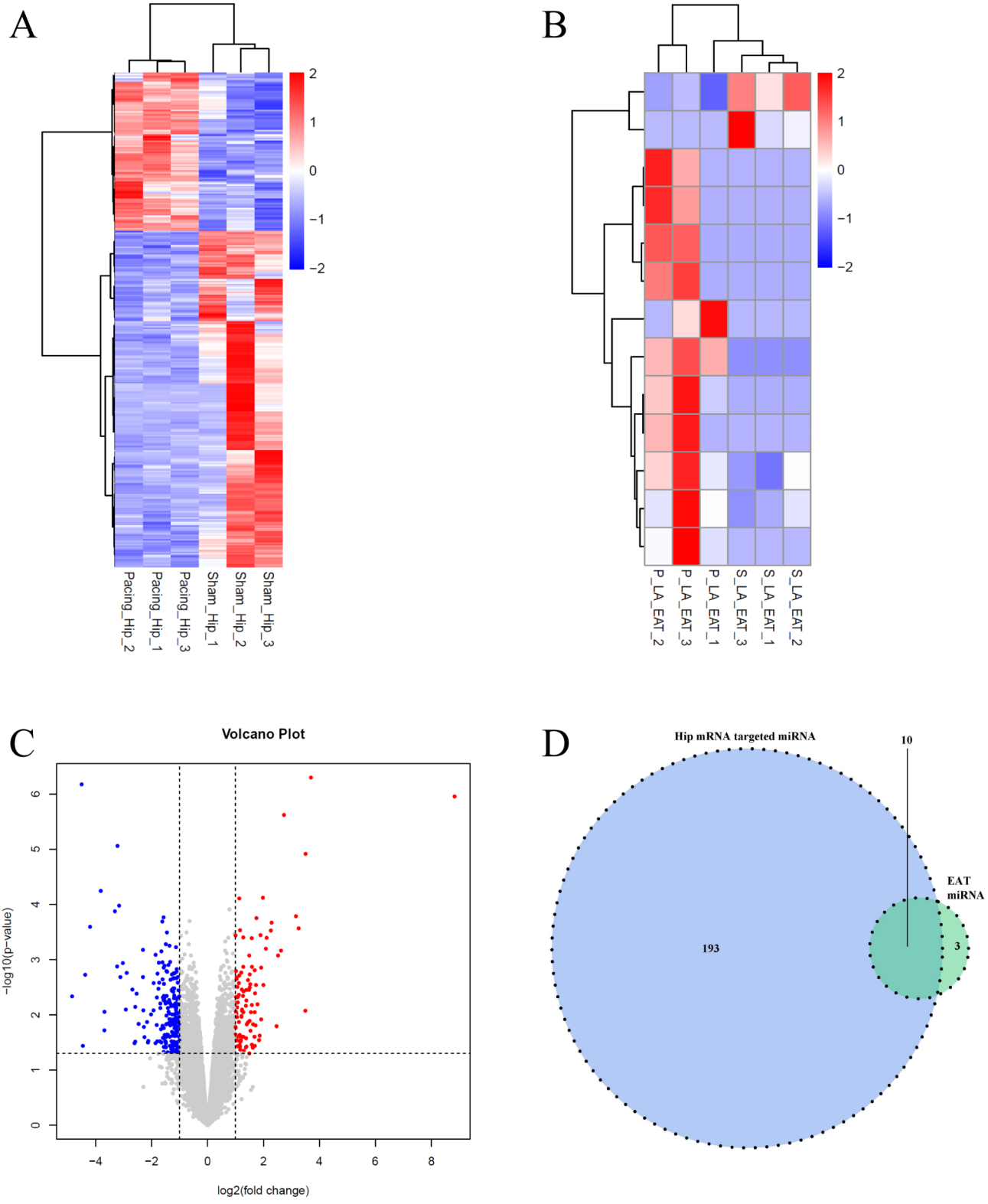

Fig. 4 RNA-seq analysis of DEGs in the canines of the sham group and pacing group. (**A**, **B**) The heatmap shows clustering of DEGs in the hippocampal tissue and EAT exosomes of the sham group and the pacing group. (**C**) Volcano plot showing significantly upregulated (red), downregulated (blue), and nonsignificant (gray) mRNAs in the hippocampus. (**D**) Venn diagram of the intersection of target miRNAs from the hippocampus and miRNAs from EAT exosomes. DEGs = differentially expressed genes; EAT = epicardial adipose tissue; Hip = hippocampus; LA = left atrium

Table 1 Hippocampal differentially expressed genes associated with microglia and their target miRNAs

mRNA Name	*P* value	Target miRNA	*P* value
IL33	0.031	cfa-miR-22e	0.047
HK2	0.018	cfa-miR-423a	0.833
HK2	0.018	cfa-miR-107	0.863
HK2	0.018	cfa-miR-103	0.703
CD14	0.015	novel-119	0.066
CD14	0.015	novel-56	0.500
CD14	0.015	cfa-miR-128	0.898
IL1B	0.005	cfa-miR-204	0.720
CCL2	0.047	novel-71	None
HSP70	0.008	None	None

Exogenous IL-33 can reverse the activation of BV2 cells induced by cfa-miR-22e

To verify the role of IL-33 in the activation of BV2 cells by cfa-miR-22e, we introduced exogenous IL-33 while treating microglial cells with cfa-miR-22e mimics and observed the expression of IBA-1 in microglia. qRT-PCR results showed that cfa-miR-22e levels in the mimics group were significantly higher than in the control, mimics NC, and cfa-miR-22e inhibitor groups (2.22±0.09 vs. 0.90±0.16, 0.93±0.05, 0.55±0.04, $P<0.001$), while no statistically significant difference was observed between the mimics group and the mimics+IL-33 group in terms of cfa-miR-22e levels. Western blot analysis revealed that IL-33 expression levels in the mimics group were significantly lower than those in the control, mimics NC, and cfa-miR-22e inhibitor groups (0.11±0.02 vs. 0.30±0.04, 0.28±0.06, 0.68±0.04, $^{*}P<0.05$, $^{**}P<0.01$, $^{***}P<0.001$), and the IL-33 levels in the mimics group were significantly lower than in the mimics+IL-33 group (0.11±0.02 vs. 0.49±0.03, $P<0.001$). Furthermore, Western blot results showed that IBA-1 levels in the mimics group were significantly higher than in the control, mimics NC, and cfa-miR-22e inhibitor groups (0.71±0.04 vs. 0.21±0.06, 0.27±0.06, 0.26±0.08, $P<0.001$), and the IBA-1 levels in the mimics group were higher than those in the mimics+IL-33 group (0.71±0.04 vs. 0.5±0.04, $P<0.05$) (Fig. 7). These results indicate that the IBA-1 elevation induced by cfa-miR-22e mimics can be reversed by exogenous IL-33.

Discussion

This study was the first to explore the effect of EAT exosomes on hippocampal microglia in AF model canines. We provide the following evidence: (1) Exosome secretion from EAT is increased in rapid atrial pacing canines, with labeled EAT exosomes distributed in the hippocampus. Microglial cells in the hippocampal tissue of rapid atrial pacing canines are significantly activated. The use of exosome inhibitors reduces EAT exosome secretion and inhibits microglial activation in the hippocampal region. (2) cfa-miR-22e exhibits a targeted relationship with IL-33. The levels of cfa-miR-22e are significantly elevated in both the EAT exosomes and hippocampal tissue of pacing canines, while IL-33 levels in the hippocampus are markedly reduced. Exosome inhibitors significantly suppress cfa-miR-22e in the hippocampus and increase IL-33 expression. (3) Exosomes derived from EAT in rapid atrial pacing canines can cross the endothelial BBB model. cfa-miR-22e downregulates IL-33, leading to an elevated expression of IBA-1. The activation of microglia is closely linked to the cfa-miR-22e/IL-33 signaling pathway.

Numerous observational studies have described an association between AF and cognitive dysfunction ranging from mild impairment to overt dementia [1, 4]. The presence of AF is associated with a 39% increased risk of CI with a lead time of years to decades [21]. However, the evidence for CI caused by AF is mainly based on clinical studies, and there is very little research on the specific molecular mechanisms involved.

The hippocampus is the main region responsible for learning and working episodic memory [22, 23], and the degree of hippocampal degeneration and damage is positively correlated with cognitive decline [24]. Previous studies have shown that AF is also a risk factor for cognitive impairment and hippocampal atrophy, even if there is no obvious stroke [7]. In our preliminary basic experiments, immunohistochemical analysis revealed no differential expression of cognitive impairment-related proteins (β-amyloid protein, tau protein) between the sham-operated group and the AF model group of canines. Moreover, no symptoms of cognitive dysfunction were observed during this experiment. Our research team has been dedicated to studying the relationship between AF and immune inflammation. After finding no direct evidence of cognitive dysfunction in the AF model, we detected statistically significant differences in hippocampal microglial markers between the sham-operated and AF groups, prompting further investigation into the mechanisms of microglial activation.

The activation of microglia can phagocytose synapses and lead to synaptic loss, which not only plays an important role in reducing hippocampal volume but is also directly related to cognitive impairment [10, 11]. In this study, we found that hippocampal microglia were significantly activated in canines with AF, as simulated by rapid atrial pacing, and that exosome inhibitors reversed the activation of hippocampal microglia. Furthermore, the fluorescence of Ad-CD63-RFP injected into the EAT of canines in the pacing group was significantly enhanced, and the fluorescence intensity of Ad-CD63-RFP and activation of microglia in the hippocampus were also significantly increased. These results suggest that the activation

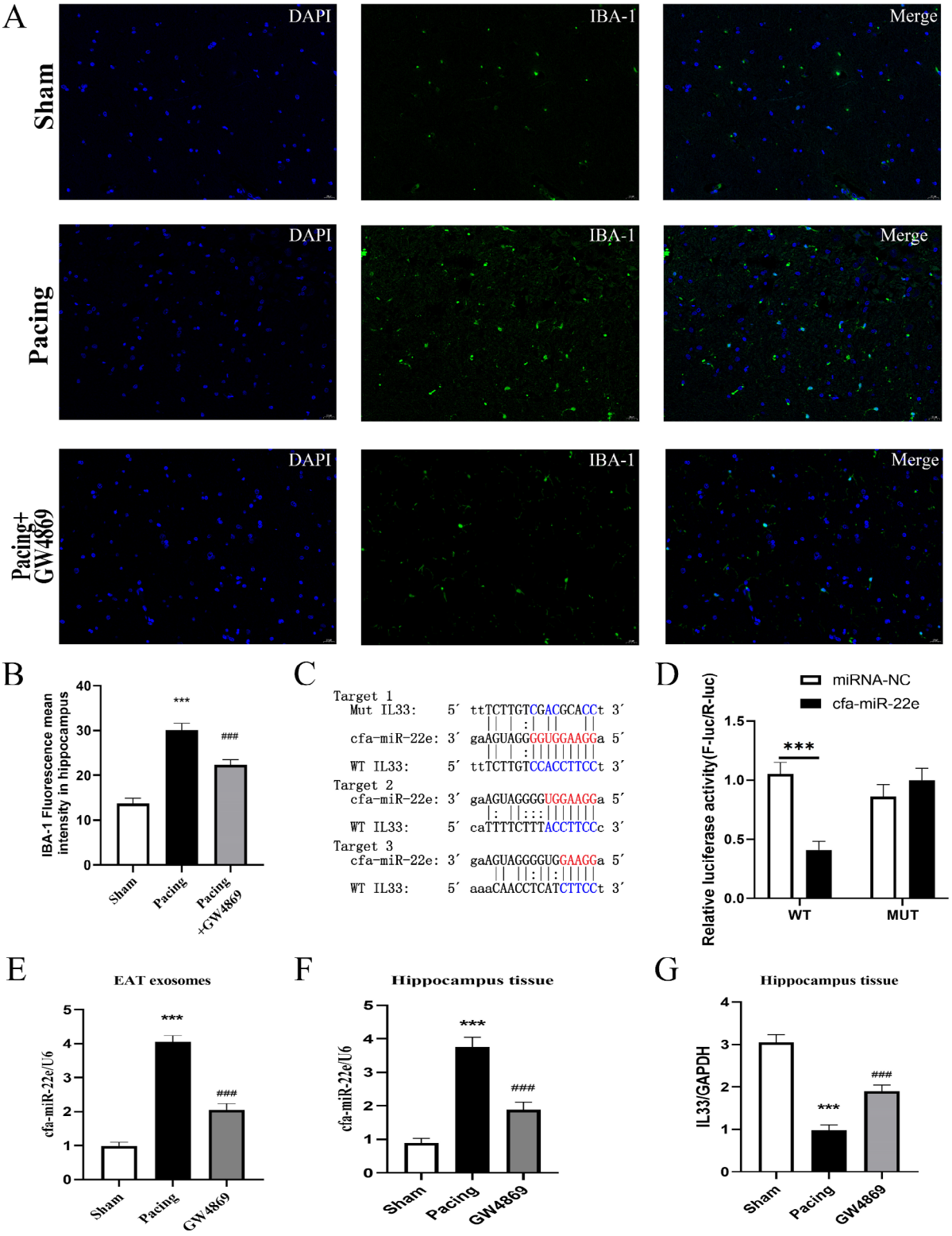

Fig. 5 cfa-miR-22e targeted IL33 and promoted microglial activation in the hippocampus. (**A**, **B**) Immunofluorescence analysis of the mean intensity of IBA1 in the hippocampus of the three groups of canines. (**C**) Target sequence of cfa-miR-22e in the wild-type (WT) IL33 3′UTR and mutated (Mut) IL33 3′UTR, as predicted by miRanda. (**D**) Measurement of firefly luciferase activity normalized to Renilla luciferase activity in 293T cells ($n=5$); *** $P<0.001$. (E, F, G) qRT-PCR was used to verify the relative levels of cfa-miR-22e in EAT exosomes and of cfa-miR-22e and IL33 in hippocampal tissue. *** $P<0.001$ versus the sham group; ### $P<0.001$ versus the pacing group

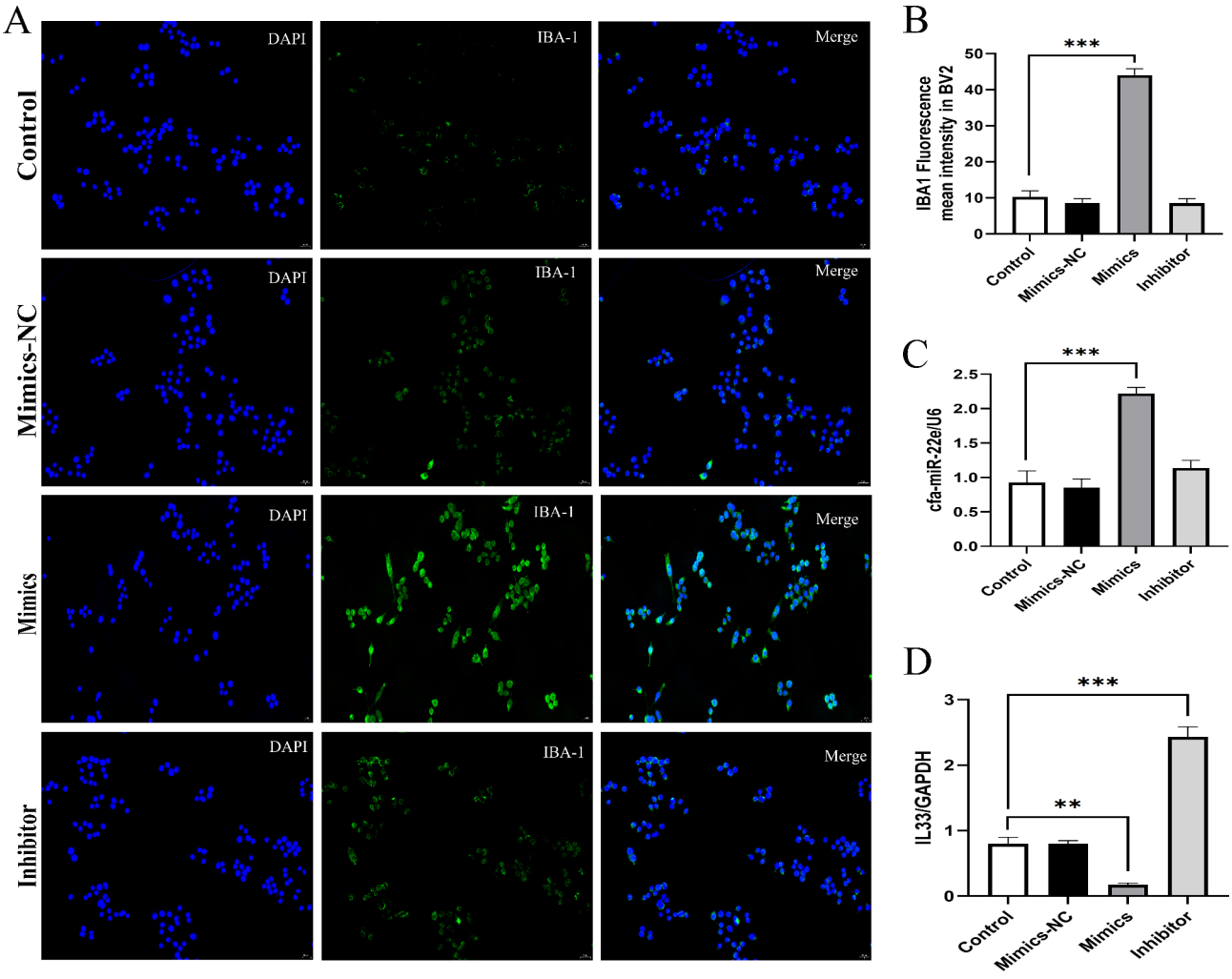

Fig. 6 BV2 cells were activated by cfa-miR-22e/IL33. (**A**) Representative images of immunofluorescence staining for IBA1 in the control, mimic-NC, cfa-miR-22e-mimics, and cfa-miR-22e-inhibitor groups of BV2 cells. (**B**-**D**) IBA1, cfa-miR-22e, and IL33 expression in different groups of BV2 cells. ** $P < 0.01$, *** $P < 0.001$

of microglia induced by rapid atrial pacing was related to the release of EAT exosomes.

Exosomes play a central role in cell-to-cell communication over short or long distances [25] and carry miRNAs to regulate cell growth and metabolism [26]. miRNAs contribute to chronic microglial inflammation in the brain and play a key role in the progression of neurological diseases [27]. Recent studies have shown that cardiovascular disease affects the nervous system through exosomes [28]. In a chronic heart failure rat model, cardiac-derived exosomes enriched in miRNA-27a, miRNA-28a, and miRNA-34a entered the brain through the BBB to promote sympathetic hyperactivity [29]. In this study, in vivo and in vitro experiments verified that EAT exosomes from pacing group canines could penetrate the BBB to activate hippocampal microglia, and GW4869 abolished these changes.

We extracted exosomes from the EAT of canines, sequenced the exosomes and hippocampal tissues, and jointly analysed the differentially expressed RNAs. Target prediction of hippocampal mRNAs using the miRanda database, followed by intersection analysis with miRNAs detected in EAT exosomes, identified 10 miRNAs with heart-brain overlap. Among the hippocampal mRNAs related to microglia, only the targeting cfa-miR-22e of IL-33 exhibited significant differential expression, prompting further investigation. Among the other heart-brain overlapping miRNAs, miR-140 was found to target 15 differentially expressed mRNAs in hippocampal tissue. Some studies suggest that SERPINE1 and SELE, among these mRNAs, are associated with microglial activation and cognitive function. However, transcriptome sequencing results showed that both SERPINE1 and SELE were downregulated in the pacing group, and miR-140 expression in EAT exosomes was also reduced

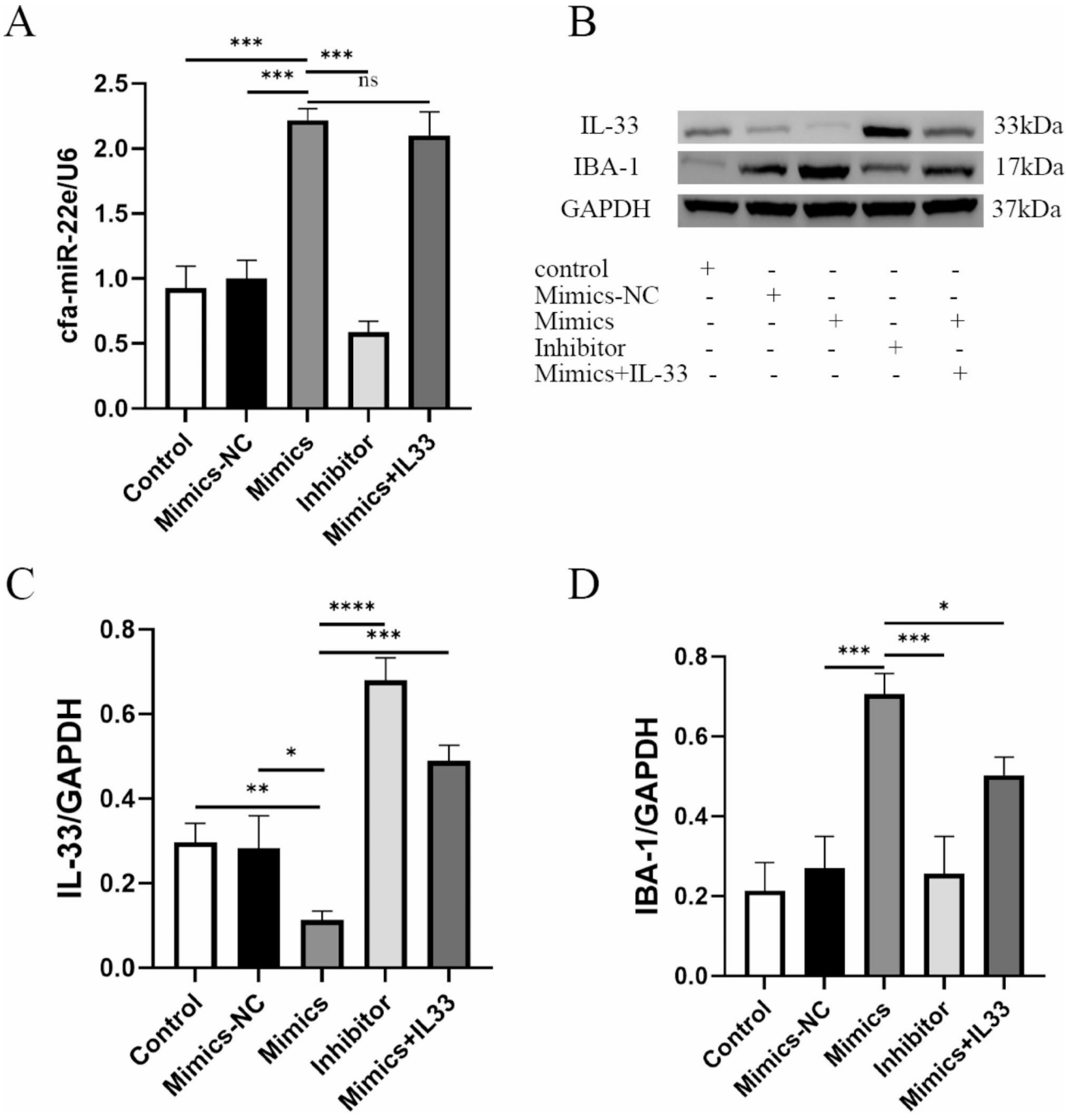

Fig. 7 Exogenous IL-33 reverses BV2 cell activation induced by cfa-miR-22e. (**A**) Real-time quantitative PCR analysis of cfa-miR-22 levels in BV2 cells. (**B**) Representative Western blot images showing the expression of IL-33 and IBA-1 in BV2 cells. (**C**, **D**) Statistical analysis of IL-33 and IBA-1 expression in BV2 cells by Western blot ($n = 3$, data are presented as mean ± SD), $^{*}P < 0.05$, $^{**}P < 0.01$, $^{***}P < 0.001$, $^{****}P < 0.0001$

in the same group. This observation contradicts the classical biological regulatory mechanism by which miRNAs typically degrade or inhibit their target mRNAs.

Xiao's research showed that the percentage of microglia in the central nervous system of IL33 knockout mice increased, microglia were activated, and the release of IL33 inhibited the activation of microglia [30]. A study by Nguyen et al. showed that IL33 mediates neuron-microglia communication and promotes hippocampal dendritic spine formation and synaptic plasticity in an experience-dependent manner; these changes are related to improvements in cognitive function. Reduced expression of IL33 in the hippocampus is associated with a progressive decrease in neuronal expression and impairment of precise memory [31]. Exogenous recombinant IL33 can significantly inhibit the expression of

proinflammatory genes in the brains of Alzheimer's disease model mice, contribute to neuroprotection, and improve hippocampal synaptic dysfunction and cognitive impairment [32].

The major findings of this study were that the level of cfa-miR-22e was significantly increased in the EAT exosomes and hippocampus of pacing group canines, and its target mRNA, IL33, was significantly downregulated in the hippocampus; however, treatment with GW4869 reversed these changes. Furthermore, we conducted cell experiments to verify the relationship between cfa-miR-22e/IL33 and BV2 cells. The results of the vitro and vivo experiments were consistent, indicating that the activation of hippocampal microglia in canines with AF was related to the regulation of cfa-miR-22e/IL33.

Limitations

This study has several limitations. First, during the experiment, we observed canine behavior and performed cranial magnetic resonance in all the canines, and we did not observe the manifestations of CI described by Dewey [33]. This may be directly related to the shorter duration of the AF model. However, we found that hippocampal microglia were significantly activated in AF canines and that the activation of hippocampal microglia was related to EAT exosomes. Whether a longer duration of atrial fibrillation models will induce cognitive dysfunction symptoms and alterations in related proteins remains to be further investigated. Second, we did not assess other indicators related to microglial activation, nor did we conduct dynamic monitoring of microglial activation at multiple time points. However, existing studies have already demonstrated the significant impact of EAT exosomes on microglial activity. Third, the dose of virus used in the canine study was based on the dose used in other studies, and no viral gradient was established, but the doses of virus we used were able to trace the presence of EAT exosomes in the hippocampus.

Conclusion

We demonstrated for the first time that the exosomes secreted by EAT in canines with AF penetrated the BBB and activated microglia in the hippocampus through the cfa-miR-22e/IL33 signalling pathway.

Acknowledgements

We thank Xi Wang, Teng Wang and Siwei Song for their technical support and experimental assistance at the Cardiovascular Research Institute of Wuhan University, Wuhan, China.

Author contributions

Xuewen W: Investigation, Validation, Software, Visualization, Writing – original draft. Yuanjia K: Investigation, Validation, Software, Writing – original draft. Zhen C: Investigation, Validation, Writing – original draft. Yuntao F: Methodology, Investigation, Validation. Yanni C: Methodology, Investigation, Validation. Dishiwen L: Investigation, Validation. Huiyu C: Investigation, Validation. Kexin G: Investigation, Validation. Yajia L: Investigation, Validation. Mei Y: Conceptualization, Supervision. Qingyan Z: Conceptualization, Supervision, Project administration.

Funding

This work was supported by the National Natural Science Foundation of China (No. 82170312 and 81970277 to Qingyan Zhao).

Data availability

The RNA sequencing data have been deposited in the NCBI GEO database under the accession number GSE240776.

Declarations

Ethics approval and consent to participate

The animal study was reviewed and approved by the Animal Care and Use Committee of Renmin Hospital, Wuhan University, under the ethical approval number WDRM 20191211. All animal experiments complied with the ARRIVE guidelines.

Consent for publication

Not applicable.

Competing interests

The authors declare no competing interests.

Author details

[1]Department of Cardiology, Renmin Hospital of Wuhan University, 238 Jiefang Road, Wuhan 430060, Hubei, China
[2]Cardiovascular Research Institute, Wuhan University, Wuhan 430060, Hubei, China
[3]Hubei Key Laboratory of Cardiology, Wuhan University, Wuhan 430060, Hubei, China
[4]Cardiovascular Department, Taihe Hospital, Hubei University of Medicine, Shiyan 442000, Hubei, China

Received: 4 March 2024 / Accepted: 20 October 2024
Published online: 09 November 2024

References

1. Rivard L, Friberg L, Conen D, Healey JS, Berge T, Boriani G, Brandes A, Calkins H, Camm AJ, Yee Chen L, Lluis Clua Espuny J, Collins R, Connolly S, Dagres N, Elkind MSV, Engdahl J, Field TS, Gersh BJ, Glotzer TV, Hankey GJ, Harbison JA, Haeusler KG, Hills MT, Johnson LSB, Joung B, Khairy P, Kirchhof P, Krieger D, Lip GYH, Løchen ML, Madhavan M, Mairesse GH, Montaner J, Ntaios G, Quinn TJ, Rienstra M, Rosenqvist M, Sandhu RK, Smyth B, Schnabel RB, Stavrakis S, Themistoclakis S, Van Gelder IC, Wang JG, Freedman B. Atrial Fibrillation and Dementia: A Report From the AF-SCREEN International Collaboration. Circulation 145 (2022) 392–409.
2. Hindricks G, Potpara T, Dagres N, Arbelo E, Bax JJ, Blomström-Lundqvist C, Boriani G, Castella M, Dan GA, Dilaveris PE, Fauchier L, Filippatos G, Kalman JM, Meir ML, Lane DA, Lebeau JP, Lettino M, Lip GYH, Pinto FJ, Thomas GN, Valgimigli M, Van Gelder IC, Van Putte BP, Watkins CL. 2020 ESC guidelines for the diagnosis and management of atrial fibrillation developed in collaboration with the European Association for Cardio-Thoracic Surgery (EACTS): the Task Force for the diagnosis and management of atrial fibrillation of the European Society of Cardiology (ESC) developed with the special contribution of the European Heart Rhythm Association (EHRA) of the ESC. Eur Heart J. 2021;42:373–498.
3. Cardiogenic Dementia. Lancet 1. (1977) 27 – 8.
4. Papanastasiou CA, Theochari CA, Zareifopoulos N, Arfaras-Melainis A, Giannakoulas G, Karamitsos TD, Palaiodimos L, Ntaios G, Avgerinos KI, Kapogiannis D, Kokkinidis DG. Atrial fibrillation is Associated with cognitive impairment, all-cause dementia, vascular dementia, and Alzheimer's Disease: a systematic review and Meta-analysis. J Gen Intern Med. 2021;36:3122–35.
5. Pendlebury ST, Rothwell PM. Prevalence, incidence, and factors associated with pre-stroke and post-stroke dementia: a systematic review and meta-analysis. Lancet Neurol. 2009;8:1006–18.
6. Kim D, Yang PS, Yu HT, Kim TH, Jang E, Sung JH, Pak HN, Lee MY, Lee MH, Lip GYH, Joung B. Risk of dementia in stroke-free patients diagnosed

with atrial fibrillation: data from a population-based cohort. Eur Heart J. 2019;40:2313–23.
7. Knecht S, Oelschläger C, Duning T, Lohmann H, Albers J, Stehling C, Heindel W, Breithardt G, Berger K, Ringelstein EB, Kirchhof P, Wersching H. Atrial fibrillation in stroke-free patients is associated with memory impairment and hippocampal atrophy. Eur Heart J. 2008;29:2125–32.
8. Moazzami K, Shao IY, Chen LY, Lutsey PL, Jack CR Jr., Mosley T, Joyner DA, Gottesman R, Alonso A. Atrial fibrillation, brain volumes, and subclinical cerebrovascular disease (from the atherosclerosis risk in communities Neurocognitive Study [ARIC-NCS]). Am J Cardiol. 2020;125:222–8.
9. Nakase T, Tatewaki Y, Thyreau B, Odagiri H, Tomita N, Yamamoto S, Takano Y, Muranaka M, Taki Y. Impact of atrial fibrillation on the cognitive decline in Alzheimer's disease. Alzheimers Res Ther. 2023;15:15.
10. Uddin MS, Lim LW. Glial cells in Alzheimer's disease: from neuropathological changes to therapeutic implications. Ageing Res Rev. 2022;78:101622.
11. Fixemer S, Ameli C, Hammer G, Salamanca L, Uriarte Huarte O, Schwartz C, Gérardy JJ, Mechawar N, Skupin A, Mittelbronn M, Bouvier DS. Microglia phenotypes are associated with subregional patterns of concomitant tau, amyloid-β and α-synuclein pathologies in the hippocampus of patients with Alzheimer's disease and dementia with Lewy bodies. Acta Neuropathol Commun. 2022;10:36.
12. Jeppesen DK, Fenix AM, Franklin JL, Higginbotham JN, Zhang Q, Zimmerman LJ, Liebler DC, Ping J, Liu Q, Evans R, Fissell WH, Patton JG, Rome LH, Burnette DT, Coffey RJ. Reassessment Exosome Composition Cell. 2019;177:428–e44518.
13. Zhang S, Yang Y, Lv X, Liu W, Zhu S, Wang Y, Xu H. Unraveling the intricate roles of exosomes in Cardiovascular diseases: a comprehensive review of physiological significance and pathological implications. Int J Mol Sci 24 (2023).
14. Shaihov-Teper O, Ram E, Ballan N, Brzezinski RY, Naftali-Shani N, Masoud R, Ziv T, Lewis N, Schary Y, Levin-Kotler LP, Volvovitch D, Zuroff EM, Amunts S, Regev-Rudzki N, Sternik L, Raanani E, Gepstein L, Leor J. Extracellular vesicles from Epicardial Fat facilitate Atrial Fibrillation. Circulation. 2021;143:2475–93.
15. Sun LL, Duan MJ, Ma JC, Xu L, Mao M, Biddyut D, Wang Q, Yang C, Zhang S, Xu Y, Yang L, Tian Y, Liu Y, Xia SN, Li KX, Jin Z, Xiong Q, Ai J. Myocardial infarction-induced hippocampal microtubule damage by cardiac originating microRNA-1 in mice. J Mol Cell Cardiol. 2018;120:12–27.
16. Tufekci KU, Eltutan BI, Isci KB, Genc S. Resveratrol inhibits NLRP3 Inflammasome-Induced pyroptosis and miR-155 expression in Microglia through Sirt1/AMPK pathway. Neurotox Res. 2021;39:1812–29.
17. Tang S, Jing H, Song F, Huang H, Li W, Xie G, Zhou J. MicroRNAs in the spinal microglia serve critical roles in Neuropathic Pain. Mol Neurobiol. 2021;58:132–42.
18. Kambayashi R, Izumi-Nakaseko H, Goto A, Tsurudome K, Ohshiro H, Izumi T, Hagiwara-Nagasawa M, Chiba K, Nishiyama R, Oyama S, Nunoi Y, Takei Y, Matsumoto A, Sugiyama A. Translational studies on Anti-atrial Fibrillatory Action of Oseltamivir by its in vivo and in vitro electropharmacological analyses. Front Pharmacol. 2021;12:593021.
19. Liu D, Yang M, Yao Y, He S, Wang Y, Cao Z, Chen H, Fu Y, Liu H, Zhao Q. Cardiac Fibroblasts Promote Ferroptosis in Atrial Fibrillation by Secreting Exo-miR-23a-3p Targeting SLC7A11. Oxid Med Cell Longev 2022 (2022) 3961495.
20. Chen CC, Liu L, Ma F, Wong CW, Guo XE, Chacko JV, Farhoodi HP, Zhang SX, Zimak J, Ségaliny A, Riazifar M, Pham V, Digman MA, Pone EJ, Zhao W. Elucidation of Exosome Migration across the blood-brain barrier model in Vitro. Cell Mol Bioeng. 2016;9:509–29.
21. Koh YH, Lew LZW, Franke KB, Elliott AD, Lau DH, Thiyagarajah A, Linz D, Arstall M, Tully PJ, Baune BT, Munawar DA, Mahajan R. Predictive role of atrial fibrillation in cognitive decline: a systematic review and meta-analysis of 2.8 million individuals. Europace. 2022;24:1229–39.
22. Hardcastle C, O'Shea A, Kraft JN, Albizu A, Evangelista ND, Hausman HK, Boutzoukas EM, Van Etten EJ, Bharadwaj PK, Song H, Smith SG, Porges EC, Dekosky S, Hishaw GA, Wu SS, Marsiske M, Cohen R, Alexander GE, Woods AJ. Contributions of hippocampal volume to Cognition in healthy older adults. Front Aging Neurosci. 2020;12:593833.
23. Banquet JP, Gaussier P, Cuperlier N, Hok V, Save E, Poucet B, Quoy M, Wiener SI. Time as the fourth dimension in the hippocampus. Prog Neurobiol. 2021;199:101920.
24. Bartsch T, Dohring J, Rohr A, Jansen O, Deuschl G. CA1 neurons in the human hippocampus are critical for autobiographical memory, mental time travel, and autonoetic consciousness. Proc Natl Acad Sci U S A. 2011;108:17562–7.
25. Saint-Pol J, Gosselet F, Duban-Deweer S, Pottiez G, Karamanos Y. Targeting and crossing the blood-brain barrier with Extracellular vesicles. Cells 9 (2020).
26. Yu X, Odenthal M, Fries JW. Exosomes as miRNA carriers: formation-function-future. Int J Mol Sci 17 (2016).
27. Karthikeyan A, Patnala R, Jadhav SP, Eng-Ang L, Dheen ST. MicroRNAs: key players in Microglia and Astrocyte mediated inflammation in CNS pathologies. Curr Med Chem. 2016;23:3528–46.
28. Duan MJ, Yan ML, Wang Q, Mao M, Su D, Sun LL, Li KX, Qu Y, Sun Q, Zhang XY, Huang SY, Ma JC, Ban T, Ai J. Overexpression of miR-1 in the heart attenuates hippocampal synaptic vesicle exocytosis by the posttranscriptional regulation of SNAP-25 through the transportation of exosomes. Cell Commun Signal. 2018;16:91.
29. Tian C, Gao L, Rudebush TL, Yu L, Zucker IH. Extracellular vesicles regulate Sympatho-Excitation by Nrf2 in Heart failure. Circ Res. 2022;131:687–700.
30. Xiao Y, Lai L, Chen H, Shi J, Zeng F, Li J, Feng H, Mao J, Zhang F, Wu N, Xu Y, Tan Z, Gong F, Zheng F. Interleukin-33 deficiency exacerbated experimental autoimmune encephalomyelitis with an influence on immune cells and glia cells. Mol Immunol. 2018;101:550–63.
31. Nguyen PT, Dorman LC, Pan S, Vainchtein ID, Han RT, Nakao-Inoue H, Taloma SE, Barron JJ, Molofsky AB, Kheirbek MA, Molofsky AV. Microglial remodeling of the extracellular matrix promotes synapse plasticity. Cell. 2020;182:388–e40315.
32. Fu AK, Hung KW, Yuen MY, Zhou X, Mak DS, Chan IC, Cheung TH, Zhang B, Fu WY, Liew FY, Ip NY. IL-33 ameliorates Alzheimer's disease-like pathology and cognitive decline. Proc Natl Acad Sci U S A. 2016;113:E2705–13.
33. Dewey CW, Davies ES, Xie H, Wakshlag JJ. Canine cognitive dysfunction: pathophysiology, diagnosis, and treatment. Vet Clin North Am Small Anim Pract. 2019;49:477–99.

Publisher's note